Arsenic Trioxide (ATO)-Induced Pyroptosis and Activation of Natural Killer Cells in Acute Myeloid Leukemia

Jia-Yin Su
First Affiliated Hospital of Sun Yat-sen University
Li-Min Zheng
Eighth Affiliated Hospital of Sun Yat-sen University
Jie-Si Luo
First Affiliated Hospital of Sun Yat-sen University
Li-Na Wang
First Affiliated Hospital of Sun Yat-sen University
Li-Bin Huang
First Affiliated Hospital of Sun Yat-sen University
Suoyu Xiang
Department of Parasitology of Zhongshan School of Medicine, Sun Yat-sen University
Cong Liang
First Affiliated Hospital of Sun Yat-sen University
Xi Sun
Department of Parasitology of Zhongshan School of Medicine, Sun Yat-sen University
Yan-lai Tang
First Affiliated Hospital of Sun Yat-sen University
Xue-qun Luo (luoxq@mail.sysu.edu.cn)
First Affiliated Hospital of Sun Yat-sen University

Research Article

Keywords: Arsenic Trioxide (ATO), Pyroptosis, Natural Killer Cells (NK Cells), Acute Myeloid Leukemia (AML)

Posted Date: April 14th, 2022

DOI: https://doi.org/10.21203/rs.3.rs-1543353/v1

Abstract

Background: The poor prognosis of acute myeloid leukemia (AML) is partly due to the immunosuppressive leukemia environment. A therapeutic approach to induce pyroptosis is promising to work on this issue. Pyroptosis, a form of inflammatory cell death, is capable to release pro-immune factors and enhance the infiltration and cytotoxicity of natural killer (NK) cells. Chemical drugs have been verified to enhance anti-tumor immunity by inducing pyroptosis. Arsenic trioxide (ATO), a clinical drug in leukemia, is reported to be effective to kill AML cells, but it's still unclear about its mechanism in AML. Our research is aimed at exploring the ATO effect on pyroptosis induction and the anti-tumor immunity of NK cells in AML.

Methods: Pyroptotic phenomenon was detected by confocal microscopy, Annexin-V / propidium iodide staining, LDH release assay, and western blotting; The release of cytokines was detected by SDS-PAGE, proteomic analysis, ELISA, etc.; AML xenograft models were established to explore the ATO effect in vivo and the anti-tumor effect of ATO treatment was identified by tumor-volume measurement, HE staining and KI67 staining; The activity of NK cells was evaluated by immunofluorescence, flow cytometric analysis, etc.; The differential expressed proteins were identified by quantitative proteomic analysis and western blotting.

Results: We first discovered that ATO induced pyroptosis in AML cells and activated caspase-3/gasdermin E (GSDME) pathway to induce pyroptosis, and enhances the release of LDH, HMGB1, and IL-1β. Moreover, we revealed that ATO treatment promoted the proliferation, tumor-infiltration, and degranulation of NK cells in AML and its leukemia microenvironment. The further proteomic clues indicate the potential mechanisms of the ATO anti-leukemia effect in vivo.

Conclusions: These findings indicate that ATO treatment induces pyroptosis via caspase-3/GSDME pathway, enhances the release of pro-inflammatory cytokines, and activates NK cells in AML. Our data identify what is to our knowledge the first clinical drug that induces pyroptosis in AML, revealing the potential anti-leukemic and pro-immune properties of ATO treatment in the leukemia microenvironment of AML, which may be beneficial in reducing the recurrence problems associated with the leukemia microenvironment.

1. Introduction

Acute myeloid leukemia (AML) is a heterogeneous clonal disorder characterized by the accumulation of somatic cytogenetic alterations in hematopoietic progenitor cells that regulate self-renewing, proliferation, and differentiation[1]. The overall long-term survival (> 5 years) rate of AML patients with therapy is only 30 to 40%[2]. The poor prognosis of AML is partly due to the damage to the immune system and tumor microenvironment (TME) in favor of immune escape[3]. As leukemia processing, NK and AML cells can develop strategies to avoid immune system recognition and allow the AML cells to propagate in TME[4]. Further studies have noted that the immunosuppressive TME and the selective loss of an immature

subset of NK cells in AML patients is probably a reason for the poor outcome[3, 5], thus it's essential to explore strategies to remodel TME and enhance the anti-tumor immunity of NK cells against AML.

Therapeutic approaches to induce pyroptosis in AML cells may be promising to achieve this goal. Pyroptosis, a form of inflammatory cell death, is executed by gasdermins. The caspases cleave gasdermins in its middle linker to release autoinhibition on its gasdermin-N fragment, which determines its pore-forming activity that is critical to the procedure of pyroptosis [6–8]. The characteristic feature of pyroptosis is the extracellular efflux due to the pores on the cell membrane, which results in the activation of antitumor immunity[9]. Since that, therapeutic strategies designed to induce pyroptosis may expand the response of immunotherapy in leukemia. NK cells are crucial cytotoxic and cytokine-producing components of the innate immune system. Sufficient evidence shows that NK cells are capable to kill acute and chronic myeloid leukemia cells[10, 11]. The expression of NK-activating ligands on AML blasts is associated with a better prognosis for AML patients[12, 13].

There is a mutually reinforcing relationship between pyroptosis and natural killer (NK) cells. On the one hand, pyroptosis has been reported to activate NK cells. The formation of pores on the cell membrane surface during pyroptosis leads to the release of damage-associated molecular pattern molecules (DAMPs) including HMGB1 and IL-18, which can stimulate anti-tumor immunity of NK cells[14]. For example, immunoproteins such as HMGB1 can participate in lymphocyte differentiation[15] and regulate NK cells activation[16]. It has been reported that gasdermin E (GSDME)-mediated pyroptosis can robustly stimulate the cytotoxicity of NK cells, which may be responsible for advantageous survival[17–19]. NK cells elaborate cytotoxicity on cancer cells via producing various cytokines, including granzymes B[20]. On the other hand, NK cell degranulation releases granzyme that can directly induce caspase-independent pyroptosis. Granzyme B (GZMB) is capable to induce GSDME-dependent pyroptosis in tumors via both directly cleaving GSDME and indirectly activating caspase-3[17], and granzyme A can induce pyroptosis through direct cleavage of GSDMB[21]. The action of granzyme allows NK cells to have a positive feedback effect on pyroptosis.

Previous study has demonstrated that chemical drugs can enhance antitumor immunity by converting apoptosis into pyroptosis[22, 23]. Arsenic trioxide (ATO) is a clinical drug with effective curative importance in acute promyelocytic leukemia (APL) [24]. It has been suggested that ATO can restore the oncogenic function of p53, which can induce the transcription of GSDME, a member of the Gasdermin family[25, 26], suggesting that ATO may be associated with pyroptosis. Besides, ATO is previously verified to enhance the NK cell cytotoxicity against APL in vitro[27]. ATO can up-regulate the NK ligands on tumor cells thereby increasing the susceptibility of cancer cells to NK cells[28]. Though ATO has been reported to be effective to kill AML cells[29], there is still a lack of mechanistic studies on the anti-leukemic effect of ATO. Our research was aimed at exploring the ATO effect on pyroptosis induction and NK cells in AML and its mechanism of action.

2. Materials And Methods

2.1. Cell culture

The MV411 (ATCC, USA) cell line was cultured in Iscove's Modified Dulbecco's Medium (IMDM, Hyclone) containing 10% fetal bovine serum (Gibco#10099141), and molm13 (DSMZ, Germany) cell line was cultured in RPMI 1640 Medium (Gibco# C11875500BT) containing 10% fetal bovine serum. The NK92-MI cell line (Procell#CL-0533) was cultured in a Special medium for NK cells (Procell, #CM-0533). All the cell lines were maintained at 37°C in a 5% CO_2 atmosphere and had been authenticated by the Cell Line Authentication Services, using Short Tandem Repeat (STR) analysis and a regular screen for Mycoplasma contamination by RT-PCR.

2.2. Treatment paradigm

AML cell lines (MV411 and MOLM13) were divided into different groups according to the dose of ATO. The control group was exposed to 1% DMSO and the ATO group was treated with 3 μM or 6 μM ATO; According to the application of ATO or Z-DEVD-FMK, AML cells were divided into ATO or ATO + DEVD groups. The ATO group was treated with 5 μM ATO, and the ATO + DEVD group was treated with both 5 μM ATO and 25 μM Z-DEVD-FMK (caspase-3 specific inhibitor) for the in vitro experiment.

2.3. Animal experiments and ethical statements

The animals in our study were approved by the Institutional Animal Care and Use Committee of The First Affiliated Hospital of Sun Yat-Sen University (No. [2021] 040). To establish nude mouse xenograft models, female nude mice (four weeks old; average weight, 15g) were obtained from Experimental Animal Laboratories (Zhuhai, China). MV411 cells (AML cell line) were resuspended in PBS (1×10^5 cells/mice) and then injected into the right foreleg of each mouse subcutaneously at an inoculation depth of 1 cm. After the tumor grew to about 100 mm^3, mice were randomly separated into 2 groups of 5 mice and then treated with either the vehicle (PBS, Gibco) or ATO (3 mg/kg) via intraperitoneal injection and their body weight was measured once per day. About 15 days after administration, all mice were sacrificed by cervical dislocation. Tumors, spleens, and livers were dissected. Tumor sizes in mice were measured every day using a digital caliper, and all tumor volumes were calculated using the following formula: volume = length × $(width)^2/2$.

2.4. Annexin V and PI staining

A total of 1×10^6 AML cells were treated with DMSO or ATO (3μM, 6μM) in the presence or absence of 25 μM Z-DEVD-FMK (caspase-3 specific inhibitor) for 24 h. The cells were then analyzed using the annexin V-FITC Apoptosis Kit (KeyGEN#KGA108) according to the manufacturer's protocol.

2.5. Cell preparation and flow cytometric analysis

Single-cell suspensions were prepared from the tumors, spleens and peripheral blood of nude mouse xenograft models washed with PBS and filtered through a cell strainer (200 μm). The mononuclear cell–

containing supernatants were obtained using 55% Percoll and OptiPrep gradient centrifugation, transferred, and washed twice before antibody staining. Single-cell suspensions were then stained with fluorochrome-conjugated monoclonal antibodies (eBioscience, USA) against the following cell surface markers: APC-conjugated CD49b and AF700-conjugated CD16. The images of all samples were acquired on a Beckman Coulter (Beckman, USA). Data were analyzed using CytExpert software.

2.6. Quantitative real-time reverse transcription PCR (qRT-PCR)

Total RNA was extracted from cells using TRIzol Reagent (Gibco, Carlsbad, CA, USA), and 1 μg total RNA (mRNA) was reverse-transcribed into cDNA using Evo M-MLV RT Premix (AG11706, Accurate Biology). The real-time qPCR was performed with SYBR Green Premix Pro Taq HS qPCR Kit (#AG11701, Accurate Biology), with three replicates set for each well. The mRNA expression relative to glyceraldehyde-3-phosphate dehydrogenase (GAPDH) was determined using the $2^{-\Delta\Delta CT}$ method. The primers were synthesized by RuiBiotech (Beijing, China) as the sequences described in Table S1.

2.7. LDH release assay and ELISA

LDH was measured using a Cytotoxicity LDH Assay Kit-WST (Dojindo#CK12) according to the manufacturer's instructions. The absorbance was calculated at 490 nm. IL-18, IL-1β, HMGB1, and GZMB were measured using a Quantitative IL-18/IL-1β/HMGB1/GZMB ELISA kit (MEIMIAN, China) according to the manufacturer's instructions. The absorbance was calculated at 450 nm. At least three replicated experiments were performed.

2.8. Nucleoplasmic separation of cellular proteins

Collect cells (500rpm, 3min), discard the supernatant and wash twice with pre-cooled PBS. Add 200 μl of CER I mixture with protease inhibitor for every 4*10^6 suspension cells, vortex for 15 s to fully lyse the cells, and left on ice for 10 min. Add CER II, vortex for 10 s, and left on ice for 1 min. Then vortex vigorously for 10 s and centrifuge at 13,200 rpm at 4°C for 5 min. The supernatant fraction was the cytoplasmic fraction of protein. The precipitated fraction was added to NER (with protease inhibitor), vortexed at high speed for 15s, and left on ice for 10min. Repeat the vortex-rest operation until the precipitate was dissolved. Add 5× loading buffer, denature the protein at 100°C for 5 min, and store at -20°C.

2.9. Sodium dodecyl sulfate-polyacrylamide gel electrophoresis (SDS-PAGE)

AML cells were treated with or without ATO and serum-free cultured for 24h. The supernatant of the culture medium was collected and concentrated 40 times. The samples with preheating (100°C for 10 min) were separated by sodium dodecyl sulfate-polyacrylamide gel electrophoresis (SDS-PAGE) on 10% agarose gels, which were peeled off and stained by Coomassie Brilliant Blue (P0017F, Beyotime).

2.10. Western blot analysis

All the proteins were extracted from cultured cells and mouse tissues by RIPA (Beyotime, Shanghai, China), using a protease inhibitor and phosphorylase inhibitor cocktail (Bimake, Shanghai, China). The protein concentration was measured via BCA Protein Assay Kit (Pierce, Rockford, IL, USA). Total cell lysate per sample was loaded on Omni-PAGE Hepes-Tris Gels (Yamei, Shanghai, China) and separated by electrophoresis. The western blot was blotted onto a piece of 0.2 um PVDF membrane using a wet transfer device (Bio-Rad). Block the blot in a 5% milk powder solution diluted in TBST (Tris-buffered saline/0.05% Tween 20), incubated with indicated antibody, and signal detected with horseradish peroxidase (HRP) -conjugated secondary antibody and enhanced chemiluminescence (ECL) detection (Bio-Rad). The following antibodies were used: anti-DFNA5/GSDME (Abcam, #ab215191), anti-cleaved-caspase-3 (Cell Signaling Technology, #9664), anti-HMGB1 (Proteintech, #10829-1-AP), anti-Granzyme B (Proteintech, #13588), anti-p38 (Novus, #96907), anti-CTSB (Cell Signaling Technology, #31718T), anti-MAPKAPK2 (Proteintech, #13949), anti-p53 (Proteintech, #60283). Equal protein loading was assessed using mouse anti-β-actin and anti-GAPDH antibodies (BOSTER, TA-09, China).

2.11. Co-culture system

AML cells were cultured in a 12-well plate in the bottom transwell (0.4μm) chamber while NK92-MIs were co-cultured in the top chamber. According to the presence or absence of treatment with ATO and the presence or absence of co-culture with MV411, they were divided into control group, MV411 + NK group, or ATO + MV411 + NK group. NK92-MI cells in the control group were treated with 0.3% as control, NK92-MI cells in the MV411 + NK group were co-cultured MV411 with NK92-MI, and NK92-MI cells in the ATO + MV411 + NK group were co-cultured MV411 with NK92-MI with 3 μM ATO added to the MV411 culture in the bottom chamber.

2.12. Cell viability assay

After the specified treatment, the ability of cell proliferation of NK-92MI cells in different groups was determined using the Cell Counting Kit-8 (CCK-8) assay reagent (Dojindo#CK04, Japan) according to the manufacturer's protocol. The absorbance was calculated at 450 nm. Three replicated experiments were performed for each well.

2.13. Hematoxylin and eosin (H&E) staining and Immunohistochemistry (IHC)

A portion of mice's xenograft tumor tissue was fixed with 4% paraformaldehyde (PH 7.4). We gradually Dewaxed as followed: Xylene I for 20 min; Xylene II for 20 min; 100% ethanol I for 5 min; 100% ethanol II for 5 min; 75% ethanol for 5 min; Stained sections with Hematoxylin solution for 3–5 min, rinsed with tap water. Then we treated the section with Hematoxylin Differentiation solution, Hematoxylin Scott Tap Bluing, and then Eosin dye for 5 min. We dehydrated as followed: 100% ethanol I for 5 min; 100% ethanol II for 5 min; 100% ethanol III for 5 min; Xylene I for 5 min; Xylene II for 5 min; Finally, we sealed with neutral gum, observed with a pathological section scanner, acquired images and analyzed them; IHC was performed on tumor tissue sections from Mouse xenograft formalin-fixed paraffin-embedded tumor

tissue sections of 4-μm thickness to analyze the expression of KI67. The sections were de-paraffinized and rehydrated. Endogenous peroxidase activity was blocked with 3% hydrogen peroxide and incubated at room temperature in darkness for 25 minutes. The sections are placed in PBS (PH7.4) and shaken on a decolorizing shaper 3 times for 5 minutes each. Then, the sections were incubated overnight at 4℃ with an anti-KI67 antibody (1:300 dilution, Servicebio). After washing off the antibodies, the sections were incubated with a secondary antibody (HRP labeled) from the corresponding species of primary antibody and incubated at room temperature for 50 minutes. Finally, diaminobenzidine substrate (DAB) was applied to sections and counterstained with hematoxylin to counterstain the nucleus for microscopic examination after resin sealing. Immunohistochemical staining intensity was semi-quantified using Image J software that compared the intensity of staining with the proportion of the stained cells. The level of KI67 expression was determined by the intensity.

2.14. Immunofluorescence (IF)

IF was performed on tumor tissue sections from Mouse xenograft formalin-fixed paraffin-embedded tumor tissue sections of 4-μm thickness to analyze the expression of Granzyme B and CD16. The following primary antibodies were used: rabbit anti-Granzyme B (Proteintech#13588, 1:200), rabbit anti-CD16 (1:200, eBioscience, USA). The sections were made and dewaxed with xylene and ethanol of different concentrations. Antigen retrieval was performed in EDTA antigen retrieval buffer (pH 8.0) and maintained at a sub-boiling temperature for 8 min and then followed by another sub-boiling temperature for 7 min. 3% hydrogen peroxide was added to the sections to block the activity of endogenous peroxidase. 3% BSA to cover the marked tissue to block non-specific binding for 30 min and then Incubating slides with primary antibody (diluted with PBS appropriately) overnight at 4 ℃. After washing, the secondary antibody (FITC) was added at room temperature for 50 min. The visualization of the nuclei was done by adding DAPI, and then the sections were mounted after adding the anti-fluorescence quencher. Images were collected by Fluorescent Microscopy. DAPI glows blue by UV excitation wavelength 330–380 nm and emission wavelength 420 nm; FITC glows green by excitation wavelength 465–495 nm and emission wavelength 515–555 nm; CY3 glows red by excitation wavelength 510–560 nm and emission wavelength 590 nm.

2.15. Label-free quantitative LC/MS proteomics analysis

The cell culture supernatants of AML cells were collected in ATO and NC groups, the AML xenograft tumors of the ATO and PBS groups were isolated from mice (n = 3 per group), and the label-free quantification proteomics analysis was performed (Novogene, China). Briefly, proteins were extracted, and the concentrations were determined by Bradford protein assay (Bio-Rad, USA). After proteins were digested with Trypsin Gold (Promega), shot-gun proteomics analyses were performed using an EASY-nLC 1200 UHPLC system (Thermo Fisher Scientific) coupled with an Orbitrap Q Exactive HF-X mass spectrometer (Thermo Fisher Scientific) operating in the data-dependent acquisition mode. Data were searched against the UniProt database for Mus musculus(85,165 sequences, downloaded 18 January 2019) database by the search engine Proteome Discoverer 2.2 (Thermo Fisher Scientific). To analyze the

protein family and pathway, the functional analysis was conducted using the interproscan program against the databases of COG (Clusters of Orthologous Groups) and KEGG (Kyoto Encyclopedia of Genes and Genomes). DEPs were used for Volcanic map analysis, cluster heat map analysis, and enrichment analysis of GO, IPR, and KEGG. The probable protein-protein interactions were predicted using the STRING server.

2.16. Statistical analysis

The statistical analysis of data was performed using GraphPad Prism 8. The comparison between the other two groups of data was analyzed by an unpaired t-test. The comparison among multiple groups was carried out by one-way analysis of variance. Body weight and tumor volume at different time points were compared using repeated-measures analysis of variance. $P < 0.05$ was considered to be significant. Graphs and error bars represent means ± SD of independent biological experiments unless stated otherwise. For all experiments, the investigators were not blinded.

3. Results

3.1. ATO induced pyroptosis in AML cells via caspase-3 / GSDME pathway

AML cell lines (MV411 and molm13) were treated with gradient doses (0, 1.5, 3, 6 μM) of ATO for 24h in the ATO group and with DMSO in the control group, followed by microscopy observation. Interestingly, we found that AML cells in the ATO group exhibited typical pyroptotic morphology, large bubbles (indicated by red arrows) emerging from the plasma membrane, and cell swelling while cells in the control group had uniform morphology with the integral cell membrane. The ratio of pyroptotic cells increased with the dose of ATO (Fig. 1a). The results of flow cytometry analyses show that the percentage of PI-positive cells increased with the dose of ATO ($P < 0.05$) (Fig. 1b). The results of cytotoxicity LDH assay and ELISA show a significant increase in LDH and IL-1β release activity of AML cells in the ATO group, which is dose-dependent on ATO (Fig. 1c-d; $P < 0.05$). Simultaneously, the western-blot results show that the protein expression levels of GSDME-N and cleaved-caspase-3 were significantly enhanced in an ATO dose-dependent manner (Fig. 1e), indicating that ATO can activate the caspase-3/GSDME pathway. Furthermore, we applied the caspase-3-specific inhibitor (Z-DEVD-FMK) at an effective dose of 25 μM in the ATO + DEVD group. The western blot results denoted that Z-DEVD-FMK could effectively inhibit caspase-3 and significantly down-regulated the protein expression of GSDME-N (Fig. 1f). As shown in Figure.1g, MV411 cells in the ATO + DEVD group had decreased ratios of cells with pyroptotic morphology (indicated by red arrows) and increased ratios of cells with the wizened but integral plasma membrane (indicated by white arrows). The flow-cytometry analysis indicated that the combination of Z-DEVD-FMK remarkably diminished cell death induced by ATO (Fig. 2h; $P < 0.05$).

3.2. ATO induced upregulation of HMGB1 expression and release into the extracellular

MV411 and molm13 cells were divided into NC and ATO groups. After treatment for 24h, the supernatants of serum-free medium were collected for electrophoretic analysis (Fig. 2a), and it was found that both MV411 and MOLM13 cells show specific protein bands in response to ATO (arrowed in Fig. 2b). Compared with the NC group, the mass spectra of 956 proteins specifically changed in the ATO group showed a 10-fold or higher increase in protein content (listed in Table S3). Importantly, the GO and KEGG analyses of 956 proteins suggest that these proteins had multiple factors closely related to immunity (Fig. 2c). Figure 2d shows that a total of 78 proteins are involved in the immune pathway, such as HMGB1. To analyze the nucleoplasmic distribution of HMGB1 protein in AML cells in response to ATO, we performed immunofluorescence co-localization and the results show that compared to the NC group, HMGB1 in the ATO group distributed more in the cytoplasm of AML cells, while the nucleus of AML cells had less HMGB1 protein (Fig.S3b). Then, the nucleoplasmic separation experiment was performed and the expression levels of HMGB1 protein were identified in the nucleus, cytoplasm, and culture supernatant of ATO-induced pyroptotic AML cells. The western-blot results show that the distribution of HMGB1 decreased in the nuclear fraction and increased in the plasmatic fraction in response to ATO treatment (Fig. 2e-f). These results suggest that ATO stimulated the migration of HMGB1 from the nucleus to the cytoplasm. Moreover, the culture supernatant was analyzed by electrophoresis, and the results show that the HMGB1 release of AML cells in the ATO group was increased compared to that of the NC group (Fig. 2g), and METTL3 as a negative control was not detected in the cell culture supernatant (Fig. 2h). Similarly, the results of ELISA and RT-qPCR show that the release of HMGB1 in the cell-culture supernatant was upregulated in the ATO group, compared with the NC group (Fig. 2i, FigS3c-d; $P < 0.05$).

3.3. ATO induced pyroptosis via caspase-3/GSDME pathway and enhanced release of DAMPs and proinflammation cytokines in vivo

The growth curve of tumor volume shows that the AML xenograft tumor progression was significantly suppressed in the ATO group compared to the control group (Fig. 3b). The results of ki67 staining and HE staining show that the areas of tumor necrosis expanded and the proliferation ability of cancer cells was inhibited in the ATO group (Fig. 3c, Fig.S4e). To detect the side effects of ATO treatment, the body weight, liver weight, and spleen weight of mice were measured and the results showed no significant difference between the ATO and control groups (Fig.S4a-d). Furthermore, the results of western blots indicated that the expression of GSDME-FL, GSDME-N, and cleaved-caspase-3 was significantly enhanced in the AML xenograft mice in the ATO group (Fig. 3d; $P < 0.05$). We also found that the protein expression of NLRP3 was higher in the AML xenograft tumors with higher expression of GSDME, demonstrating that the NLRP3 expression levels were positively correlated with the expression levels of GSDME-N. Furthermore, the results of ELISA shows that the secretion levels of DAMPs (LDH and HMGB1) and proinflammation cytokines IL-1β were enhanced after ATO treatment (Fig. 3e-f; $P < 0.05$).

3.4. ATO activated the proliferation and GZMB-degranulation capacity of NK cells in vitro and in vivo

To explore whether ATO-induced pyroptosis could enhance the immune activity of NK cells, we measured the behavior of NK-92-MI alone and co-cultured with MV411 cells pre-treated or untreated with ATO for 24h. CCK-8 assay shows that cell proliferation of NK-92MIs in the ATO + MV411 + NK group was statistically significant up-regulated compared to the MV411 + NK group (Fig. 4a; $P < 0.05$). Flow-cytometry analysis of annexin V and propidium iodide staining indicated that the cell death of MV411 cells that were co-cultured with NK cells treated with ATO was notably improved compared with those untreated with ATO (Fig. 4b; $P < 0.05$). The release of GZMB in the supernatants of NK92-MI cells was examined by ELISA and found that it was increased when cocultured with AML cells treated with ATO in a dose-dependent manner (Fig. 4c; $P < 0.05$). The increased degranulation of GZMB could be inhibited by Z-DEVD-FMK (caspase-3 specific inhibitor) (Fig. 4d; $P < 0.05$). For in vivo experiments, flow-cytometry analysis of NK ($CD16^+CD49b^+$) cells staining shows that the percentages of NK cell population were significantly increased in tumors, spleens, and peripheral blood of mice in the ATO group compared with the control group, suggesting that the proliferation and tumor infiltration capacity of NK cells could be up-regulated by ATO (Fig. 4e, S5b-c; $P < 0.05$). Results of immunofluorescence staining show that the expression levels of GZMB were up-regulated in tumor-infiltrating NK cells in the ATO group (Fig. 4f; $P < 0.05$). Analysis of western blots shows the expression level of granzyme B in the ATO group was higher than that in the control group (Fig. 4g; $P < 0.05$). Moreover, the secretion level of granzyme B in the serum of the ATO group was higher than that of the control group (Fig. 4h; $P < 0.05$).

3.5. Proteomics analysis of AML xenograft tumor

To further uncover the underlying mechanisms of the anti-leukemia effect of ATO, differentially expressed proteins (DEPs) of the AML xenograft tumors were explored by Label-Free-based quantitative proteomics analyses. A total of 4618 proteins were identified by proteomic quantitative analysis. According to the standard of DEPs with a fold change of over 1.5-fold as well as $p < 0.05$, we screened 63 up-regulated proteins and 20 down-regulated proteins in the ATO group versus the PBS group (Table S4). The DEPs were displayed as a volcano plot (Fig. 5a). KEGG pathway analysis depicted that the immune system was the one enriched with the largest number of DEPs (Fig. 5b). As for the signaling pathway involved in the ATO effect, KEGG pathway analysis shows that the upregulated DEPs were principally enriched in the MAPK cell death signaling pathway, NOD-like receptor signaling pathway, MAPK signaling pathway, Th17 cell differentiation, etc. (Fig. 5c). Among these, the MAPK cell death signaling pathway and NOD-like receptor signaling pathway were most significantly altered. Their targets included Cathepsin B, Mitogen-activated protein kinase 14 (p38), p53, and NOD-like receptor protein 3 (NLRP3), which were further validated by western blots (Fig. 3f, 5e).

4. Discussion

Here, we have discovered that ATO treatment can induce pyroptosis via caspase-3/GSDME pathway and activate the anti-tumor immunity of NK cells in AML for the first time. First, we observed an interesting phenomenon that AML cells treated with ATO exhibited a typical pyroptosis morphology in a dose-dependent manner. As important features of pyroptotic cells[30], the upregulated percentages of PI^+ cells and LDH release also confirmed that ATO induced pyroptosis in AML cells. Furthermore, previous studies have shown that active caspase-3 (cleaved-caspase-3) can cleave GSDME-FL at its middle linker, liberating the N terminal of gasdermin E (GSDME-N) domain to form pores on the plasma membrane, leading to pyroptosis[22, 23]. As shown in our results of in vitro and in vivo experiments, ATO-induced pyroptosis resulted from caspase-3 cleavage of GSDME, which could be significantly inhibited by caspase-3 inhibitor. Moreover, as inflammatory cell death, pyroptosis not only alters the internal environment of cancer cells but also the extracellular environment due to the rapid pore formation and the release of intracellular DAMPs and proinflammation cytokines [30]. A recent study has found that GSDME-N can stimulate the expression of NLRP3, which is an inflammasome that enables the mature proinflammation cytokine IL-1β to release into the extracellular space[31]. Our in vivo experiments show that the expression levels of NLRP3 were upregulated in the group with higher expression of GSDME-N in AML xenograft tumors and the release levels of IL-1β in serum were increased as well, which indicates that the expression of NLRP3 was positively correlated with the expression level of GSDME-N, which enhanced the release of proinflammation cytokine IL-1β consequently. Previous research has confirmed that IL-1β can amplify the local or systemic immune response[32, 33]. In addition, gasdermins activation permits not only the release of pro-inflammatory cytokines but also the release of DAMPs, which can activate anti-tumor immune responses, thus eliciting long-term efficacy of chemotherapeutic drugs[31, 34]. Thus, we address the damage-associated molecular patterns (DAMPs) released by ATO-induced pyroptotic cells using proteomic analysis and found that ATO stimulated AML cells to release immune-related proteins. Among them, high-mobility group box 1 (HMGB1) is one of the most critical DAMP related to pyroptosis and is available to invigorate immunity[34, 35]. HMGB1 is a chromatin-binding protein that is mainly distributed in the nucleus and partially in the cytoplasm. We have identified that ATO induced up-regulation of HMGB1 gene expression and stimulated HMGB1 to migrate from the nucleus to the cytoplasm and release extracellularly. Previous studies have illustrated that HMGB1 is functioning to recruit inflammatory cells and mediate signals between natural killer (NK) cells and other immune cells[36].

Our data suggest that ATO treatment stimulated the release of DAMPs and proinflammatory cytokines in vivo, which may mediate immune cell recruitment in the tissue[37–39]. What kind of immune cells were recruited or activated by ATO treatment? Recent studies have demonstrated that the tumor-suppressive function of GSDME is correlated with pyroptosis-dependent activation of killer cytotoxic lymphocyte[17]. It has been demonstrated that NK cells can target and kill AML cells[10], and the NK cell activation is positively linked to better outcomes for patients undergoing chemotherapy in AML[12]. Therefore, we further explored the ATO effect on the potential of NK cells and found that ATO could enhance the

proliferation and tumor infiltration of NK cells both in vitro and in vivo. The secretion level of GZMB was previously found to strengthen the cytotoxicity of NK cells against AML cells[13, 20, 40]. Our results also show that ATO treatment can promote the expression and release of granzyme B (GZMB) in the tumor microenvironment (TME) of AML, indicating that ATO may enhance the cytotoxicity of NK cells against AML cells via stimulating the degranulation of GZMB. Moreover, GZMB is capable to activate caspase-independent pyroptosis in cancer cells by directly cleaving GSDME at the same site as caspase 3 [17], which can magnify inflammation signals and recruit more immune cells in TME[41]. Our data have demonstrated that ATO could both activate caspase-3/GSDME pyroptosis pathway and improve the expression and release of GZMB, implying that ATO-induced pyroptosis may be positive feedback by activating NK cells to release more GZMB.

To further investigate the mechanism of the anti-leukemia activity of ATO treatment in vivo, label-free quantitative proteome analysis was applied to explore the DEPs of the AML xenograft tumors. The results of KEGG analysis suggest that ATO treatment mainly mobilizes the immune system in AML xenograft mice, and the MAPK signaling pathway and NOD-like receptor signaling pathway was significantly activated. Previous studies have found that these two signaling pathways were crucial to the initiation of pyroptosis and induction of cancer cell death[26, 42, 43]. The DEPs in the two signaling pathways included p38, p53, cathepsin B (CTSB), and NLRP3. Our data confirmed that their protein expression levels were up-regulated consistently. As previously reported, p53 can be uniquely activated by HMGB1 and p38[44, 45], and the activation of p53 can in turn promote GSDME transcription[26, 42, 43], which may convert apoptosis into pyroptosis when it is highly expressed in cancer cells[22]. Our data have shown that ATO could stimulate the release of HMGB1 and up-regulate the expression levels of p38 and p53, indicating that the upregulation of p53 by ATO treatment is probably a consequence of the promotion of p38 and HMGB1, thus promoting GSDME transcription to induce pyroptosis. Moreover, it's believed that DAMPs (HMGB1 and LDH) can induce lysosome destabilization and stimulate the release of CTSB[46], and CTSB can directly activate the inflammasome NLRP3, which leads to the maturation and release of IL-1β[47, 48]. In addition, NLRP3 can also be activated by GSDME-N and facilitate the maturation and release of IL-1β[49]. As shown in our results, ATO-induced pyroptosis resulted from the caspase-3 cleavage of GSDME and liberation of GSDME-N to form pores on the plasma membrane. Meanwhile, ATO improved the expression of NLRP3 and CTSB in the AML xenograft tumors and enhanced the release of both HMGB1, LDH and IL-1β simultaneously. Based on these evidences, we tentatively put forward the potential mechanism of the ATO anti-leukemia effect in AML as shown in Fig. 6: DAMPs (HMGB1 and LDH) released from ATO-induced pyroptotic cells could not only disrupt the lysosomes to release CTSB but also uniquely activate the expression of p38 and p53, which in turn promoted GSDME transcription and positively feedback pyroptosis in the surrounding AML cells. Subsequently, CTSB and GSDME-N could synergistically activate NLRP3 inflammasome to stimulate the maturation and release of IL-1β. DAMPs and pro-inflammatory cytokines released from pyroptotic cells may further recruit NK cells and activate the degranulation of GZMB, which could directly cleave GSDME to induce pyroptosis in AML cells in a caspase-independent manner.

Nevertheless, certain limitations were presented in this research. First, our study has put forward that ATO could both activate caspase-3/GSDME pyroptosis pathway and the anti-tumor immunity of NK cells. Though it is already reported that pyroptosis can ignite the immune response of NK cells[17], it's remained to explore the association between ATO-induced pyroptosis and the activation of the immune response of NK cells; Moreover, our study has shown that ATO could enhance the expression and release of GZMB in NK cells. Although GZMB has been previously proved to cleave GSDME directly, further studies are needed to investigate whether ATO-induced pyroptosis is positive feedback by GZMB in AML; In addition, as revealed by proteomic clues, our results indicate that the activation of MAPK signaling pathway and NOD-like signaling pathway may candidate in the anti-AML effect of ATO, but more work will be needed to confirm their participation in the anti-AML effect of ATO.

Conclusions

Our in vitro and in vivo study has indicated that ATO treatment induces pyroptosis in AML cells via caspase-3/GSDME pathway and enhances the release of DAMPs (LDH and HMGB1) and pro-inflammatory cytokine IL-1β. Moreover, we have illustrated that ATO treatment promotes the proliferation and GZMB degranulation of NK cells in AML, as well as upregulating the infiltration and GZMB expression of NK cells in the leukemia microenvironment. The further proteomic clues indicate that ATO mainly activates the immune system in vivo, and its anti-tumor effect may be related to the activation of p38, p53, and CTSB. Our data identify the first clinical drug that induces pyroptosis in AML, revealing the potential anti-leukemic and pro-immune properties of ATO treatment in AML and its leukemia microenvironment, which may be beneficial in reducing the recurrence problems associated with the leukemia microenvironment.

Declarations

Supplementary information

Supplementary information accompanies this paper in additional files.

Ethical approval and consent to participate

The in vivo assay using nude mice were approved by the Institutional Animal Care and Use Committee of The First Affiliated Hospital of Sun Yat-Sen University (No. [2021] 040).

Consent for publication

All patients involved in our study obtained written consent for publication.

Availability of data and materials

The datasets used and analyzed during the current study are available within the manuscript and its additional files.

Competing interests

The authors declare no conflict of interest.

Funding

This study was supported by grants from the Science and Technology Planning Project of Guangdong Province, China [Grant No. A2021352], the Scientific Research Project of Guangdong Traditional Chinese Medicine [Grant No. A20201056], and the Guangdong Basic and Applied Basic Research Foundation [Grant No.2020A1515010282].

Authors' contributions

SJY, ZLM, and LXQ contributed to conceptualization; SJY, ZLM, WLN, LC, and HLB contributed to formal analysis; SJY, ZLM, and XSY contributed to the investigation; SJY, ZLM, LJS, LXQ, SX, and TYL contributed to methodology and resources; SJY contributed to writing—original draft; LXQ, LJS, ZLM, SX, and TYL contributed to writing—review and editing. All authors read and approved the final manuscript.

Acknowledgments

Not applicable.

References

1. Fröhling, S., et al., *Genetics of myeloid malignancies: pathogenetic and clinical implications*. J Clin Oncol, 2005. 23(26): p. 6285–95.
2. Ley, T.J., et al., *Genomic and epigenomic landscapes of adult de novo acute myeloid leukemia*. N Engl J Med, 2013. 368(22): p. 2059–74.
3. Mirfakhraie, R., et al., *Treatment Failure in Acute Myeloid Leukemia: Focus on the Role of Extracellular Vesicles*. Leuk Res, 2021. 112: p. 106751.
4. Ruggeri, L., et al., *Effectiveness of donor natural killer cell alloreactivity in mismatched hematopoietic transplants*. Science, 2002. 295(5562): p. 2097–100.
5. Baragaño Raneros, A., C. López-Larrea, and B. Suárez-Álvarez, *Acute myeloid leukemia and NK cells: two warriors confront each other*. Oncoimmunology, 2019. 8(2): p. e1539617.
6. Shi, J., et al., *Cleavage of GSDMD by inflammatory caspases determines pyroptotic cell death*. Nature, 2015. 526(7575): p. 660–5.
7. Shi, J., W. Gao, and F. Shao, *Pyroptosis: Gasdermin-Mediated Programmed Necrotic Cell Death*. Trends Biochem Sci, 2017. 42(4): p. 245–254.
8. Ding, J., et al., *Pore-forming activity and structural autoinhibition of the gasdermin family*. Nature, 2016. 535(7610): p. 111–6.

9. Chen, X., et al., *Turning up the heat on non-immunoreactive tumors: pyroptosis influences the tumor immune microenvironment in bladder cancer*. Oncogene, 2021. 40(45): p. 6381–6393.
10. Yan, Y., et al., *Antileukemia activity of a natural killer cell line against human leukemias*. Clin Cancer Res, 1998. 4(11): p. 2859–68.
11. Schlegel, P., et al., *NKG2D Signaling Leads to NK Cell Mediated Lysis of Childhood AML.* J Immunol Res, 2015. 2015: p. 473175.
12. Mastaglio, S., et al., *Natural killer receptor ligand expression on acute myeloid leukemia impacts survival and relapse after chemotherapy*. Blood Adv, 2018. 2(4): p. 335–346.
13. Carlsten, M. and M. Järås, *Natural Killer Cells in Myeloid Malignancies: Immune Surveillance, NK Cell Dysfunction, and Pharmacological Opportunities to Bolster the Endogenous NK Cells*. Front Immunol, 2019. 10: p. 2357.
14. Shao, F., *Gasdermins: making pores for pyroptosis*. Nat Rev Immunol, 2021. 21(10): p. 620–621.
15. Gergues, M., et al., *Neuroimmune/Hematopoietic Axis with Distinct Regulation by the High-Mobility Group Box 1 in Association with Tachykinin Peptides*. J Immunol, 2020. 204(4): p. 879–891.
16. Coppola, A., et al., *Activation of Peripheral Blood Mononuclear Cells and Leptin Secretion: New Potential Role of Interleukin-2 and High Mobility Group Box (HMGB)1*. Int J Mol Sci, 2021. 22(15).
17. Zhang, Z., et al., *Gasdermin E suppresses tumour growth by activating anti-tumour immunity*. Nature, 2020. 579(7799): p. 415–420.
18. Maltez, V.I., et al., *Inflammasomes Coordinate Pyroptosis and Natural Killer Cell Cytotoxicity to Clear Infection by a Ubiquitous Environmental Bacterium*. Immunity, 2015. 43(5): p. 987–97.
19. Meng, J., et al., *Pyroptosis-related gene mediated modification patterns and immune cell infiltration landscapes in cutaneous melanoma to aid immunotherapy*. Aging (Albany NY), 2021. 13(21): p. 24379–24401.
20. Bossi, G. and G.M. Griffiths, *Degranulation plays an essential part in regulating cell surface expression of Fas ligand in T cells and natural killer cells*. Nat Med, 1999. 5(1): p. 90–6.
21. Zhou, Z., et al., *Granzyme A from cytotoxic lymphocytes cleaves GSDMB to trigger pyroptosis in target cells*. Science, 2020. 368(6494).
22. Rogers, C., et al., *Cleavage of DFNA5 by caspase-3 during apoptosis mediates progression to secondary necrotic/pyroptotic cell death*. Nat Commun, 2017. 8: p. 14128.
23. Wang, Y., et al., *Chemotherapy drugs induce pyroptosis through caspase-3 cleavage of a gasdermin*. Nature, 2017. 547(7661): p. 99–103.
24. Lengfelder, E., W.K. Hofmann, and D. Nowak, *Impact of arsenic trioxide in the treatment of acute promyelocytic leukemia*. Leukemia, 2012. 26(3): p. 433–42.
25. Chen, S., et al., *Arsenic Trioxide Rescues Structural p53 Mutations through a Cryptic Allosteric Site*. Cancer Cell, 2021. 39(2): p. 225–239.e8.
26. Masuda, Y., et al., *The potential role of DFNA5, a hearing impairment gene, in p53-mediated cellular response to DNA damage*. J Hum Genet, 2006. 51(8): p. 652–664.

27. Alex, A.A., et al., *Arsenic Trioxide Enhances the NK Cell Cytotoxicity Against Acute Promyelocytic Leukemia While Simultaneously Inhibiting Its Bio-Genesis*. Front Immunol, 2018. 9: p. 1357.
28. Kim, J.Y., et al., *Induction of NKG2D ligands and subsequent enhancement of NK cell-mediated lysis of cancer cells by arsenic trioxide*. J Immunother, 2008. 31(5): p. 475–86.
29. Liu, X.J., et al., *Arsenic trioxide induces autophagic degradation of the FLT3-ITD mutated protein in FLT3-ITD acute myeloid leukemia cells*. J Cancer, 2020. 11(12): p. 3476–3482.
30. Ruan, J., *Structural Insight of Gasdermin Family Driving Pyroptotic Cell Death*. Adv Exp Med Biol, 2019. 1172: p. 189–205.
31. Zhou, B. and D.W. Abbott, *Gasdermin E permits interleukin-1 beta release in distinct sublytic and pyroptotic phases*. Cell Rep, 2021. 35(2): p. 108998.
32. Broz, P., P. Pelegrín, and F. Shao, *The gasdermins, a protein family executing cell death and inflammation*. Nat Rev Immunol, 2020. 20(3): p. 143–157.
33. Wang, Y.Y., X.L. Liu, and R. Zhao, *Induction of Pyroptosis and Its Implications in Cancer Management*. Front Oncol, 2019. 9: p. 971.
34. Ahmed, A. and S.W.G. Tait, *Targeting immunogenic cell death in cancer*. Mol Oncol, 2020. 14(12): p. 2994–3006.
35. Krysko, D.V., et al., *Immunogenic cell death and DAMPs in cancer therapy*. Nat Rev Cancer, 2012. 12(12): p. 860–75.
36. Lotze, M.T. and K.J. Tracey, *High-mobility group box 1 protein (HMGB1): nuclear weapon in the immune arsenal*. Nat Rev Immunol, 2005. 5(4): p. 331–42.
37. Murao, A., et al., *Release mechanisms of major DAMPs*. Apoptosis, 2021. 26(3–4): p. 152–162.
38. Lamkanfı, M., et al., *Inflammasome-dependent release of the alarmin HMGB1 in endotoxemia*. J Immunol, 2010. 185(7): p. 4385–92.
39. Hou, L., et al., *NLRP3/ASC-mediated alveolar macrophage pyroptosis enhances HMGB1 secretion in acute lung injury induced by cardiopulmonary bypass*. Lab Invest, 2018. 98(8): p. 1052–1064.
40. Reusing, S.B., et al., *CD16xCD33 Bispecific Killer Cell Engager (BiKE) as potential immunotherapeutic in pediatric patients with AML and biphenotypic ALL*. Cancer Immunol Immunother, 2021. 70(12): p. 3701–3708.
41. Tan, Y., et al., *Pyroptosis: a new paradigm of cell death for fighting against cancer*. J Exp Clin Cancer Res, 2021. 40(1): p. 153.
42. Düzgün, M.B., et al., *A Bioinformatic Approach for the Identification of Molecular Determinants of Resistance/Sensitivity to Cancer Thermotherapy.* Oxid Med Cell Longev, 2019. 2019: p. 4606219.
43. Jayaraman, L., et al., *High mobility group protein-1 (HMG-1) is a unique activator of p53*. Genes Dev, 1998. 12(4): p. 462–72.
44. Chae, W.O. and G.D. Kim, *Dioscin Decreases Breast Cancer Stem-like Cell Proliferation via Cell Cycle Arrest by Modulating p38 Mitogen-activated Protein Kinase and AKT/mTOR Signaling Pathways*. J Cancer Prev, 2021. 26(3): p. 183–194.

45. Lin, H., et al., *Iron(II)-Polypyridyl Complexes Inhibit the Growth of Glioblastoma Tumor and Enhance TRAIL-Induced Cell Apoptosis*. Chem Asian J, 2018. 13(18): p. 2730–2738.
46. Kumar, S. and M. Dhiman, *Inflammasome activation and regulation during Helicobacter pylori pathogenesis*. Microb Pathog, 2018. 125: p. 468–474.
47. Chevriaux, A., et al., *Cathepsin B Is Required for NLRP3 Inflammasome Activation in Macrophages, Through NLRP3 Interaction*. Front Cell Dev Biol, 2020. 8: p. 167.
48. Hoegen, T., et al., *The NLRP3 inflammasome contributes to brain injury in pneumococcal meningitis and is activated through ATP-dependent lysosomal cathepsin B release*. J Immunol, 2011. 187(10): p. 5440–51.
49. Mundy-Bosse, B.L., et al., *MicroRNA-29b mediates altered innate immune development in acute leukemia*. J Clin Invest, 2016. 126(12): p. 4404–4416.

Figures

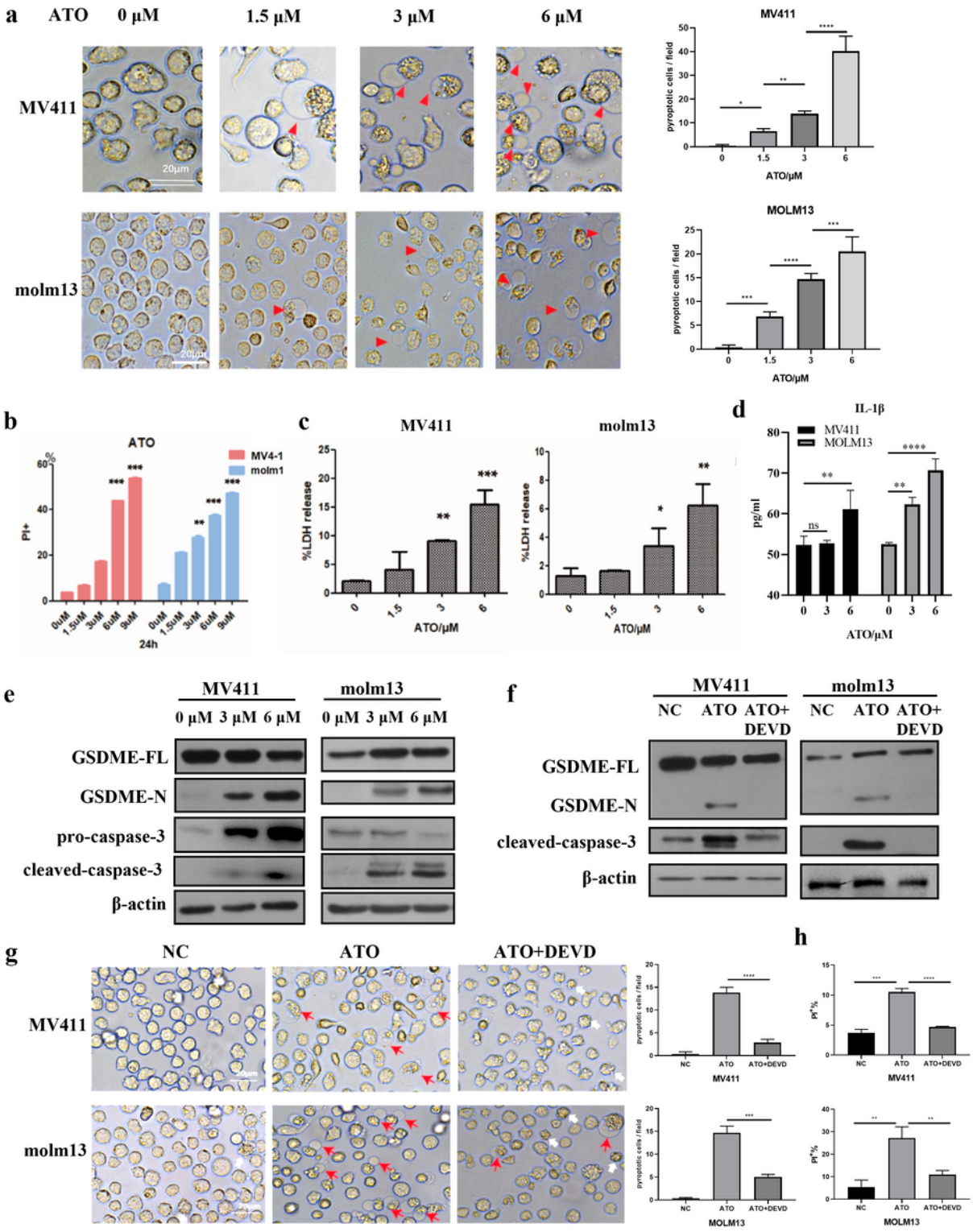

Figure 1

ATO induced pyroptosis in AML cells via the activation of caspase-3/GSDME pathway. AML cell lines (MV411, molm13) were treated with ATO at indicated concentrations (0, 1.5, 3, 6 μ mol/L) for 24h. As for ATO or ATO+DEVD groups, the ATO group was treated with 5 μ M ATO, and the ATO+DEVD group was treated with both 5 μ M ATO and 25 μ M Z-DEVD-FMK (caspase-3 specific inhibitor) for 24h. (a) Representative microscopic images of AML cells after ATO treatment for 24h (m=400×). The red arrows

denote the typical balloon in the membrane of pyroptosis cells. Scale bar 20μm. (b) Flow cytometry analysis of the percentage of Annexin-V+ PI+ AML cells after ATO treatment. (c) The release of LDH of AML cells was measured by cytotoxicity LDH assay. (d) The release levels of IL-1β were detected by ELISA in the supernatants of AML cells. (e-f) The expression levels of full-length GSDME (GSDME-FL), the N-terminal of GSDME (GSDME-N), and caspase-3 were detected by western blot in AML cells. (g) Representative microscopic images of AML cells in ATO and ATO+DEVD groups (m=400×). The red arrows denote the typical balloon in the membrane of pyroptotic cells. The white arrows denote apoptotic cells. Scale bar 20μm. (h) Flow cytometry analysis of the percentage of Annexin-V+ PI+ AML cells. All the data is presented as mean ± SD from at least 3 independent experiments. ns: not significant ($P > 0.05$), *$P < 0.05$, **$P < 0.01$, ***$P < 0.001$, and ****$P < 0.0001$, vs. control using one-way ANOVA.

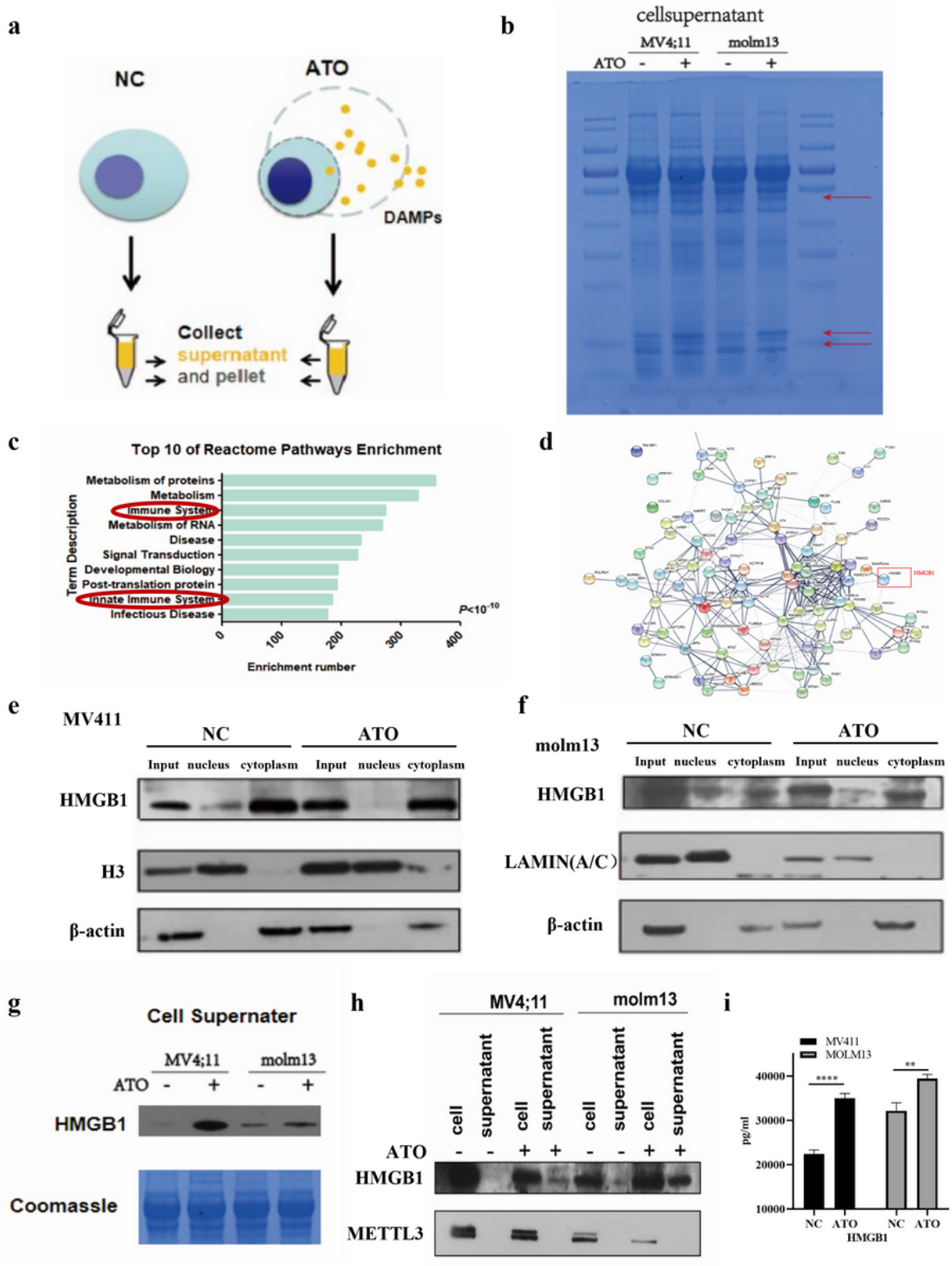

Figure 2

ATO induced upregulation of HMGB1 expression and release into the extracellular. (a) Schematic diagram of the experiment of cell-culture supernatant collection from the ATO and NC groups. (b) The gel image of Coomassie brilliant blue staining to detect the differentially expressed proteins in cell-culture supernatant of AML cells in the two groups (red arrows point to specific electrophoretic bands of ATO group) (c) Top10 Reactome pathways enrichment in proteomic analysis. (d) Functional enrichment analysis of the

interaction networks among the differentially expressed proteins that are involved in the immune system. (e-f) The expression levels of HMGB1 in the nucleus and cytoplasm were separately detected by western blot in AML cells. H3 and LAMIN(A/C) were applied as the intranuclear reference and β-actin was applied as the cytoplasmic reference. (g) The protein release levels of HMGB1 in the supernatants of AML cells in the two groups. (h) The expression levels of HMGB1 and METTL3 in AML cells and the cell supernatants. (i) The release levels of HMGB1 in the cell supernatants were measured by ELISA. ****P < 0.0001, vs. control using t-test.

Figure 3

ATO induced pyroptosis via caspase-3/GSDME pathway and enhanced release of DAMPs and cytokines in vivo. 3mg/kg ATO or PBS was injected intraperitoneally into AML xenograft mice in the ATO group and the control group once per day. After 15 days, serum and transplanted tumors were collected. (a) Schematic representation of the establishment and drug treatment of AML xenograft nude mice in the ATO group and the control group. (b) The average tumor volume (mm3) curve of the two groups was measured every day in the period of drug treatment. (c) Quantitative analysis of the immunohistochemical staining of KI67. Scale bars 100μm. (d) The relative protein expression levels of GSDME-FL, GSDME-N, cleaved-caspase-3, and NLRP3 were detected by western blot in AML xenograft tumor of the two groups. (e) The release levels of LDH and HMGB1 in the serum of AML xenograft mice in the two groups were measured by ELISA. (f) The release levels of IL-1β in the serum of AML xenograft mice in the ATO group and the control group were measured by ELISA. ns: not significant (P > 0.05), *P < 0.05, **P < 0.01, ***P < 0.001, and ****P < 0.0001, vs control using t-test.

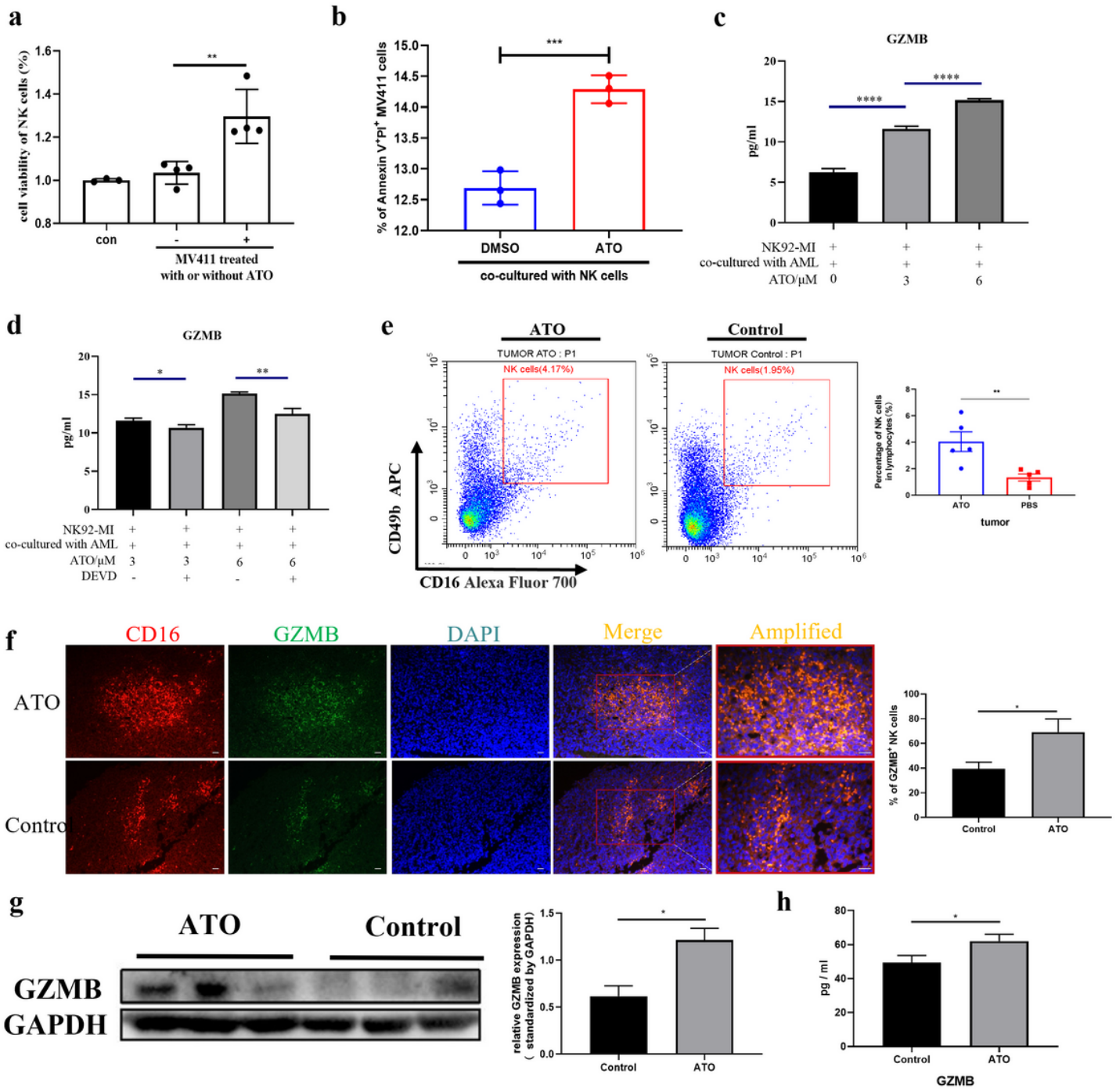

Figure 4

ATO activated the proliferation and GZMB-degranulation capacity of NK cells in vitro and in vivo. For in vitro experiments, NK92-MI cells in the control group were treated with 0.3% as control, and NK92-MI cells in the MV411+NK group were co-cultured MV411 with NK92-MI, and NK92-MI cells in the ATO+MV411+NK group were co-cultured MV411 with NK92-MI with 3μM ATO treatment. For in vivo experiments, 3mg/kg ATO or PBS was injected intraperitoneally into AML xenograft mice in the ATO group and the control group once per day. After 15 days, AML xenograft tumors and serum were collected. (a) Examination of cell viability of NK92-MI cells in the control group and the co-culture groups.

NK92-MI cells in the co-culture groups were co-cultured with MV411s pre-treated with DMSO or 3μM ATO; NK92-MI cells in the control group were treated with DMSO without co-culture with MV411 cells. (b) Flow cytometry analysis of the percentage of Annexin-V+ PI+ MV411 cells in the control group and the ATO group. MV411 cells in the two groups were respectively co-cultured with NK92-MI cells in the exposure of DMSO or 3μM ATO for 24h. (c-d) The release levels of granzyme B (GZMB) in the supernatants of NK92-MI cells. (e) Tumor cells were stained with anti-mouse CD49b-APC and anti-mouse CD16-AF700 antibodies and analyzed by flow cytometry. FMO controls were obtained by omitting anti-mouse CD49b-APC antibody or anti-mouse CD16-AF700 antibody. Analysis of FMO controls for NK cells shows that omitting anti-mouse CD49b-APC antibody or anti-mouse CD16-AF700 antibody did not significantly change the frequency of positive cells for the other marker, confirming the validity of the gating strategy. (f) Representative images of immunofluorescence staining of AML xenograft tumors in the ATO group and the control group, indicating co-localization of CD16 (red) with GZMB (green). Cell nuclei were counterstained with DAPI (blue). Scale bar 50μm. (g) Gel image of GZMB was detected by western blot in AML xenograft tumor of the two groups. (h) The release levels of GZMB in the serum of AML xenograft mice in two groups were measured by ELISA. All the data is presented as mean ± SD from at least 3 independent experiments. ns: not significant ($P > 0.05$), *$P < 0.05$, **$P < 0.01$, ***$P < 0.001$, and ****$P < 0.0001$, vs. control using t-test or one-way ANOVA.

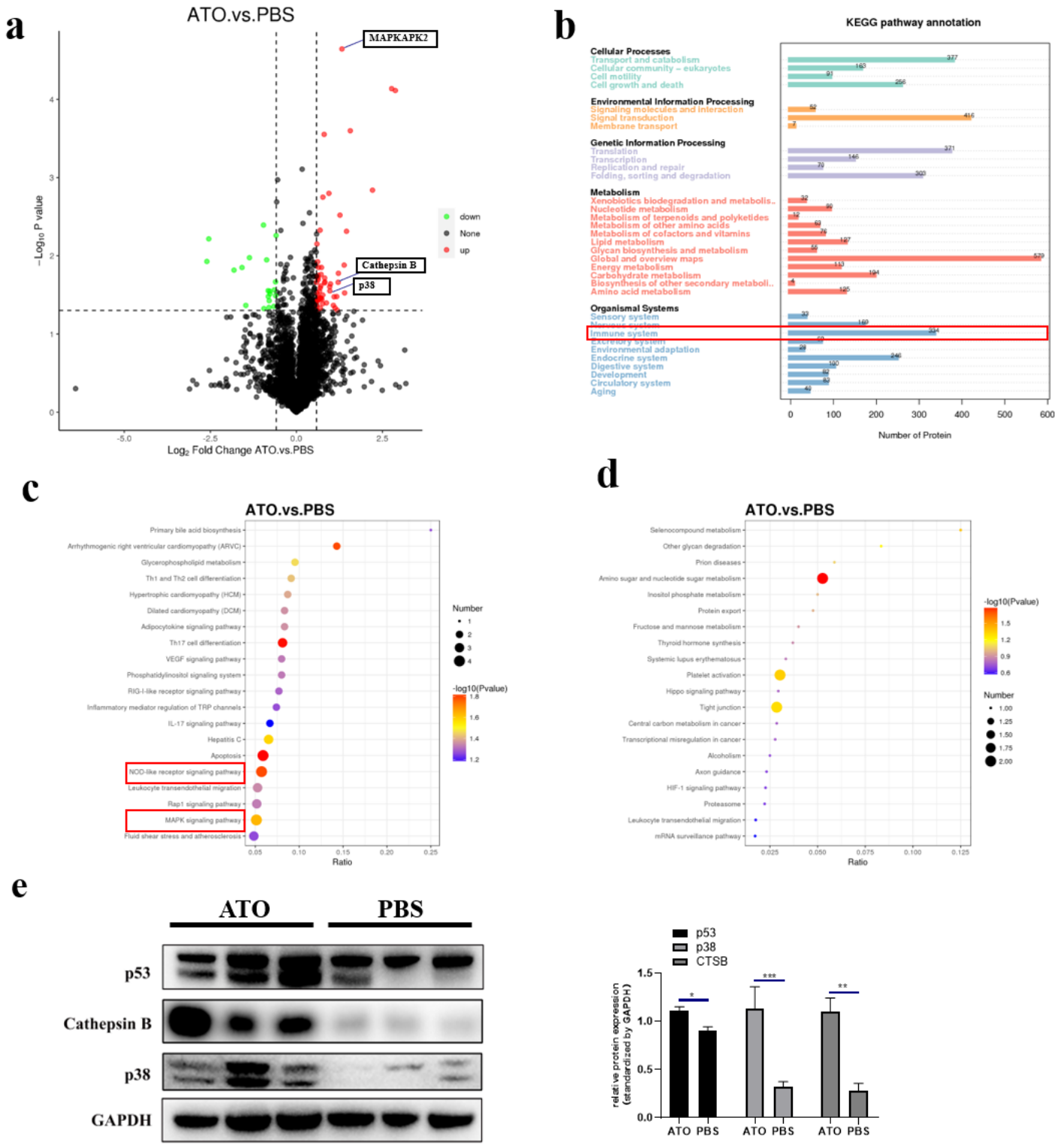

Figure 5

Proteomics analysis of AML xenograft tumor. (a) Volcano plots of proteins under- and over-expressed in AML xenograft tumor. Green dots represented down-regulated proteins, red dots meant up-regulated proteins, and gray dots show proteins with no statistically significant difference between the ATO group versus the control (PBS) group. (b) The number of differentially expressed genes on each pathway of KEGG. (c) KEGG analysis of up-regulated proteins. (d) KEGG analysis of down-regulated proteins. (e) The

expression levels of cathepsin B, p38, and p53 of tumor tissue were measured by western blots. The data are expressed as the mean ± SD. ns: not significant (P > 0.05), *P < 0.05, **P < 0.01, ***P < 0.001, and ****P < 0.0001, vs control using two-way ANOVA.

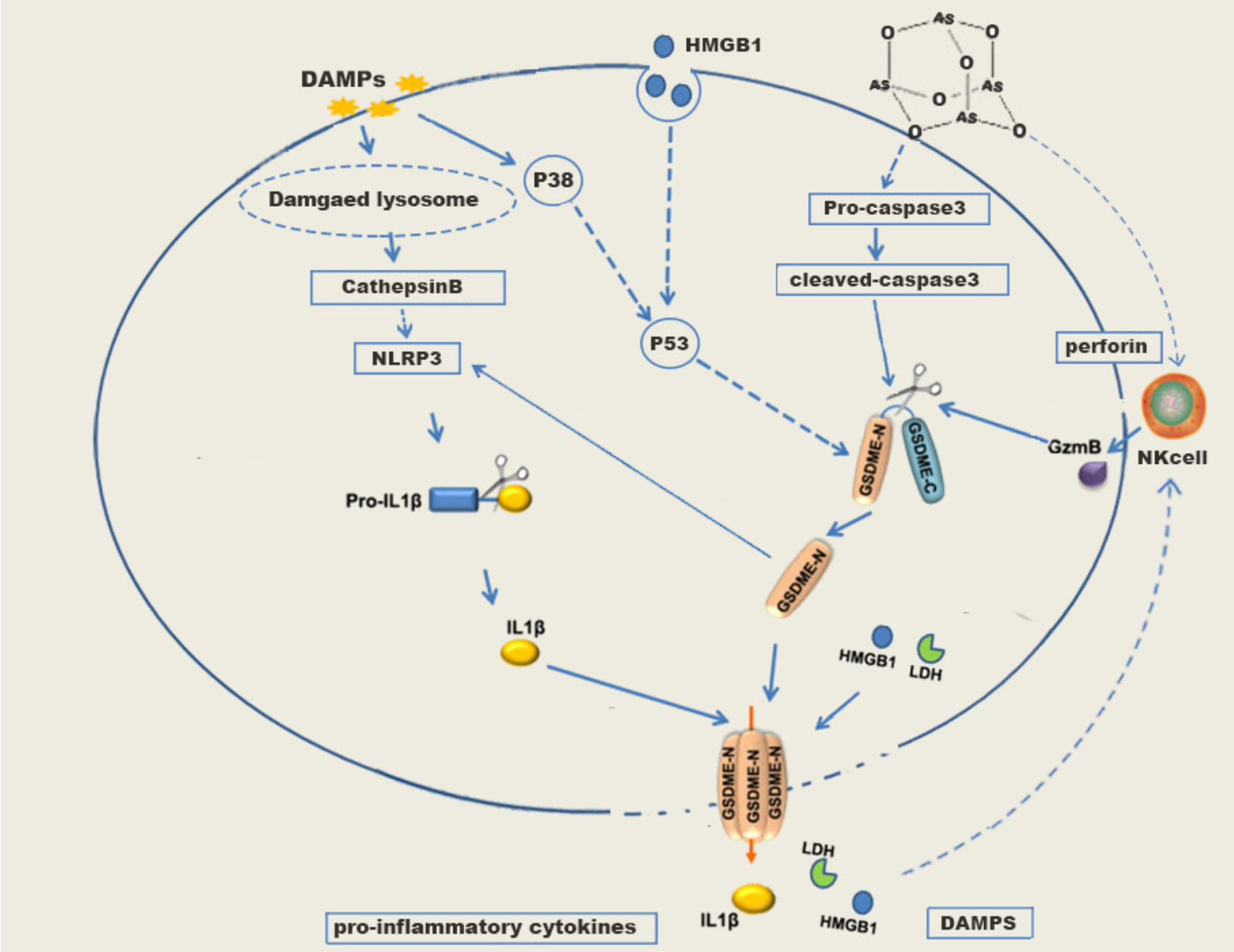

Figure 6

Potential mechanisms of ATO anti-leukemia effect in AML xenograft mice. ATO induced pyroptosis in AML cells via caspase-3/GSDME and GZMB/GSDME pathways, liberating GSDME-N to form pores in the plasma membrane. DAMPs (HMGB1 and LDH) released from the pores could disrupt the lysosomes of adjacent AML cells to release CTSB, and also uniquely activate the expression of p38 and p53, which in turn promoted GSDME transcription. Subsequently, CTSB and GSDME-N could synergistically activate NLRP3 inflammasome to stimulate the maturation and release of IL-1β. DAMPs and pro-inflammatory cytokines released from pyroptotic cells may further recruit NK cells and activate the degranulation of GZMB, which could directly cleave GSDME to induce pyroptosis in AML cells in a caspase-independent manner.

Supplementary Files

This is a list of supplementary files associated with this preprint. Click to download.

- SupplementaryMaterialJHO.docx